Factors for Improvements of Catalytic Activity of Zirconium Oxide-Based Oxygen-Reduction Electrocatalysts

Journal of The Electrochemical Society, **160** (2) F162-F167 (2013)
0013-4651/2013/160(2)/F162/6/$28.00 © The Electrochemical Society

Factors for Improvements of Catalytic Activity of Zirconium Oxide-Based Oxygen-Reduction Electrocatalysts

Yoshiro Ohgi,[a,c] Akimitsu Ishihara,[a,*] Koichi Matsuzawa,[a,*] Shigenori Mitsushima,[a,*] Ken-ichiro Ota,[a,*,z] Masashi Matsumoto,[b,*] and Hideto Imai[b,*]

[a]*Chemical Energy Laboratory, Yokohama National University, Yokohama 240-8501, Japan*
[b]*NISSAN ARC Ltd., Yokosuka 237-0061, Japan*

Partially oxidized zirconium carbonitrides (Zr-CNO) were evaluated as a non-precious-metal cathode used for polymer electrolyte fuel cells. The zirconium-oxide-based catalysts were prepared from zirconium carbonitrides under controlled oxygen partial pressures from 10^{-2} to 10^{-18} atm at 1000°C. The ORR activity of Zr-CNO showed a volcano-like tendency against the degree of oxidation (DOO). We found a significant lattice-parameter decrease for highly active Zr-CNOs, and this could be ascribed for the formation of oxygen- and zirconium-vacancies in monoclinic ZrO_2. On the other hand, carbon originated from starting materials was deposited on the surface of Zr-CNOs during the partial oxidation process. We also found that the oxygen content on the surface of highly active Zr-CNOs was drastically decreased when the amount of carbon significantly decreased during partial oxidation processes. This result indicates that the deposited carbon acted as a strong reduction agency. From XPS and XRD analyzes, there is a linear relationship between the ORR current and amount of oxygen vacancy formed in monoclinic phase. Therefore, we believe that oxygen vacancy formed in monoclinic phase could act as active sites for the ORR.
 [DOI: 10.1149/2.079302jes]

Manuscript submitted September 28, 2012; revised manuscript received November 27, 2012. Published December 13, 2012.

Polymer electrolyte fuel cells (PEFCs) are efficient and clean electrochemical power generation devices that produce electricity from H_2 and O_2 gases. Platinum-based oxygen reduction reaction (ORR) catalysts are used as the best catalyst for cathodes of PEFCs at present. Its high cost and poor availability, however, makes the development of non-noble metal catalysts highly desirable. While many studies have been done to develop non-platinum cathode catalysts for PEFCs, such as cobalt- or iron-based macrocyclic complexes (N_4-chelate type such as phtalocyanines, porphyrins, and tetraazaanulens),[1–3] metal chalcogenides ($Mo_xRu_ySe_z$, Ru_xX_y (where X = S, Se, and Te)),[4–8] and carbon-based catalysts,[9–11] these compounds are, actually, unstable in acidic and oxidizing atmosphere, and less-stable than that of platinum based cathode catalysts.[11–17]

In contrast, we have been focusing on the materials' stability to sever cathode conditions, viz., strong acidic and corrosive environments, and have developed the group 4 and 5 metal-oxide-based catalysts that have high ORR activities that are comparable to that of platinum, simultaneously exhibiting highly tolerant behaviors for the PEFC cathode condition.[18–24] The results of our studies on transition-metal-oxide-based ORR catalysts have suggested that the best ORR activity is obtained when transition-metal carbonitrides, such as ZrC_xN_y, TaC_xN_y, NbC_xN_y, are partially oxidized. Since the transition metal oxides themselves show no remarkable ORR activity, carbon and/or nitrogen that are included in the starting materials should play a role in emergence and enhancement of ORR activity of oxide-based ORR catalysts.

Zirconia -known as a valve metal- have extensively been studied because they are useful material in current technologies with many applications, such as solid electrolytes for automobile exhaust catalysts, oxygen gas sensors, and solid oxide fuel cells.[25–28] Since physical and chemical properties of zirconium oxides strongly depend on the crystalline structure, the crystal structure of the transformations of considerable technical interest. There are three polymorphisms for zirconia: monoclinic, tetragonal and cubic phases. Zirconium dioxide is normally monoclinic at room temperature, but undergoes a reversible martensitic phase transformation at about 1200°C to a tetragonal structure.[29,30] The so-called partially stabilized zirconia, which are typically two-phases cubic and tetragonal or single-phase tetragonal, are of importance for mechanical and structural application. The introduction of vacancies by substituting portion of oxygen atoms with carbon and nitrogen atoms also stabilized the tetragonal and cubic structure.[31–33] Disorder and defects as oxygen vacancy should be important in stabilizing the cubic and tetragonal structure of zirconia.

Previously, we reported that the partial oxidation process significantly improves catalytic activity of the ORR if zirconium carbonitrides were used as a starting material. We considered that the formation of oxygen-vacancies might be possible origin of the enhancement of the ORR activity.[18] Intrinsic oxygen vacancies were thermodynamically formed at equilibrium. The driving force of defect formation reaction is oxygen partial pressure, and thus, the density of oxygen vacancies should be depended on oxygen partial pressure. Therefore, in this paper, we studied the effective formation of oxygen-vacancy-defects by controlling oxygen pressure and their relationship with the ORR activity and also crystalline structures. In addition, in this research we paid special care for unwanted ORR contribution or redox current arisen from carboneous materials used as a current collector and a catalyst-support electrode. By mounting catalysts directly on a gold electrode without carbon blacks, we eliminated unwanted electrochemical contributions.

Experimental

Synthesis of electrocatalysts.— An appropriate amount of zirconium oxide and carbon powders were mixed, and the mixture was heated at 1800°C under nitrogen atmosphere to synthesize zirconium carbonitrides (Zr-CN) as a starting material.[18]

Partial oxidation was performed with a heat-treatment of the Zr-CN powders at 1000°C for 20 hours under oxygen partial pressure P_{O2} from 10^{-2} to 10^{-18} atm using oxygen partial pressure controller SiOC-200S2 (STLab, Japan) with a gas flow rate of 200 cm^3 min^{-1} in an alumina tube furnace (KT-3 × 14-VP, Koyo Thermo Systems, Japan) to prepare partially oxidized zirconium carbonitride powders. Commercial ZrO_2 (Wako Pure Chemicals Co., Japan) was calcined at 900°C under pure oxygen for 24 hours, and compared with partially oxidized Zr-CNO, as a reference of stoichiometric ZrO_2. The structure of calcined ZrO_2 was determined as monoclinic phase with stoichiometric chemical composition by high resolution XRD.

Electrochemical measurements.— At around 0.5–0.6 V near onset potential for ORR, there is a redox potential of surface functional group on carbon black like quinon/hydroquinone.[34] In a previous work, GC rod and Ketjen Black EC300J were used for a substrate and an electrical conducting material.[18] In this report, however, we do not use carbonaceous material as electrical conductive additive and substrate to eliminate the influence of the surface functional group on carbon. Instead, we used a gold plate as a substrate that treated with

*Electrochemical Society Active Member.
[c]Present address: Kumamoto Industrial Research Institute, Kumamoto, 862-0901, Japan
[z]E-mail: ken-ota@ynu.ac.jp

king acid and masked using non-conductive tape (active surface area: 0.25 cm^2, TKK, Japan). The catalyst ink was made by dispersing the catalyst in 1.0 mL of distilled water. The obtained ink was dropped on a gold plate with the Zr-CNO of ca. 8 mg cm^{-2} and covered with 12 μL of 0.5 wt% recast Nafion solution. Electrochemical measurements were conducted with three-electrode cell in oxygen or nitrogen saturated 0.1 mol dm^{-3} (M) H_2SO_4 at 30°C using PS08 potentiostat (TOHO Technical Research, Japan). A reversible hydrogen electrode (RHE) and a GC plate were used as a reference and a counter electrode, respectively. Before the catalytic activity measurements, the electrode surface was cleaned by using cyclic voltammetry scans under nitrogen at a scan rate of 50 mV s^{-1} from 0.05 to 1.2 V with 100 cycles in 0.1 M H_2SO_4 at 30°C. Then, the catalytic activity for the ORR was measured by a cyclic voltammetry from 1.2 to 0.2 V at a sweep rate of 5 mV s^{-1} in oxygen or nitrogen saturated 0.1 M H_2SO_4 at 30°C. The ORR current (i_{ORR}) was determined by subtracting the current under nitrogen from that under oxygen. We defined the onset potential for the ORR (E_{ORR}) as the electrode potential at i_{ORR} = −0.002 μA cm^{-2}. A current density was based on the geometric surface area of the working electrode. Here we identified for some sample dominant rate-determining step at higher potential is charge-transfer processes using static and rotating measurement. Thus, we will discuss ORR activity with E_{ORR} and i_{ORR} at 0.85 V measured by only static measurement.[35]

Characterization.— High-resolution synchrotron X-ray powder diffraction analyzes were performed at room temperature by using the large Debye-Scherrer optical system which installed at the BL19B2 beam line in SPring-8 with an imaging plate (IP) as a detector. The sample was loaded into a ϕ0.1 mm quartz-glass capillary. The wavelength of incident X-ray was 0.70033 Å. The X-ray diffraction intensities were obtained with a 0.01° step from 3 to 78° in 2θ. Synchrotron X-ray powder diffraction data were refined by using Rietveld analysis. Rietveld refinement uses known atomic structure to model the phase components present. This refinement allows the refinement of atomic parameters through least squares analysis until the calculated pattern, generated by the model, agrees with the experimental pattern. Rietveld analysis can yield accurate and reproducible quantitative results.[36] All the necessary structural information (symmetry, dimensions of the unit cell, and position of atoms) was gathered from existing databases and entered as the initial parameters. With all this information, Rietveld refinement was performed with the help of a RIETAN-FP software,[37] and VESTA software for visualization of crystalline structure.[38] The purpose of Rietveld refinement is to tune the unit cell dimensions to obtain the best agreement between simulation and synchrotron X-ray powder diffraction measurement: this optimization is done in iterative cycles. The refinements were carried out with lattice parameter and site occupancy.

The weight changes during oxidation process were monitored with TG-DTA (Thermo plus EVO TG-DTA 8120, Rigaku, Japan). The sample of ca. 20 mg was loaded into platinum pans and heated to 1400°C with rate of temperature increase of 20°C min^{-1} in pure oxygen flowing at a rate of 200 mL min^{-1}.

Raman spectroscopy was performed under ambient conditions with a 532 nm laser (excitation light source: Nd: YVO_4 laser) using micro-Raman system (NRS-1000, JASCO Corp.) for each lasting 180 s, from 500 to 2000 cm^{-1}. The laser beam was focused on the powder with a 100×lens, analysis area of ca. 1 μm in diameter. The laser beam power at the specimen was 0.2 mW μm^{-2}.

Observed spectra were analyzed by fitting the experimental data with five bands. The two main bands are: the D ("Defect") band (Lorentzian at ca. 1345–1360 cm^{-1}) and the G ("Graphite") band (Lorentzian at 1580–1600 cm^{-1}). Three additional bands were required to accurately fit the experimental Raman spectra. According to Sadezky et al.,[39] these three bands are attributed to: (i) amorphous carbon (Am band, Gaussian at 1490–1525 cm^{-1}), sp^3 carbon (P band, Lorentzian at 1150–1190 cm^{-1}) and (iii) another band accounting for structural disorder (D′ band, Lorentzian at ∼1620 cm^{-1}) which is observed as a shoulder on the G band. During the fit, the peak position of the P band was fixed at 1180 cm^{-1} (a value used by Sadezky et al.[39]), while the positions of Am band (between 1520 and 1540 cm^{-1},) and D′ band was (between 1610 and 1620 cm^{-1}) were varied. No boundary condition was given to peak positions of G and D bands. The values reported for all parameters described above are the average from all data acquisitions (two minimum) of each sample.

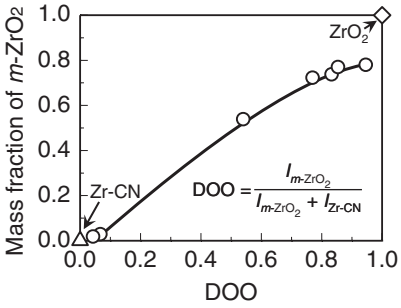

Figure 1. Relationship between degree of oxidation (DOO) and mass fraction which is simulated from XRD patterns for Zr-CNO system. The definition of DOO for Zr-CNOs is given in the inset.

Surface elemental analysis of the catalysts was performed by using X-ray photoelectron spectroscopy (XPS) with a PHI Quantera SXM instrument (ULVAC-PHI Inc., Japan). The Al Kα line (1486.6 eV) was chosen as the X-ray source. Narrow-scan photoelectron spectra were recorded for Zr3d, C1s, N1s and O1s; the elements detected in the catalysts. Thirty scans were necessary for Zr3d, forty scans for C1s, N1s and O1s. The peak of the Au $4f_{7/2}$ at 84.0 eV in the Au 4f spectrum was used to correct for surface charging up

Definition of degree of oxidation.— Degree of oxidation (DOO) was defined by using intensities of XRD patterns for the specific reflections. The starting material Zr-CN and the oxidized ZrO_2 phases coexisted. ZrO_2 has three phases: monoclinic as stable phase, tetragonal and cubic as metastable phases. For Zr-CNOs system, we observed both monoclinic and cubic phases as discuss below. Now we define the DOO for Zr-CNOs which consists of Zr-CN and monoclinic ZrO_2 phases as,

$$\mathrm{DOO} = \frac{I_{m-\mathrm{ZrO_2}}}{I_{m-\mathrm{ZrO_2}} + I_{\mathrm{ZrCN}}} \quad [1]$$

by using integrated intensity of 111 reflections of cubic (*c*) Zr-CN and $11\bar{1}$ and 111 reflection of monoclinic (*m*) ZrO_2.

Results and Discussion

DOO versus mass fraction of oxide phase ratio.— Figure 1 shows relationship between degree of oxidation and mass fraction of *m*-ZrO_2 which was simulated from actual XRD patterns for Zr-CNOs system. Mass fraction contains only *m*-ZrO_2. Correlation curve between the mass fraction and DOO for *m*-ZrO_2 is slightly convex upward as is the case with Ta-CO and Ta-NO systems.[35] Even in different oxide based material, thus, DOO as a parameter help us understanding a characteristic of oxide phase ratio and should express qualitatively same meaning of the formed phase during partial oxidation.

ORR activity.— Figure 2 shows voltammograms of Zr-CN/Au plate, Zr-CNO/Au plate, and ZrO_2/Au plate systems (DOO = 0.0, 0.83, 1.0) in 0.1 mol dm^{-3} at 30°C with scan rate of 5 mV s^{-1}. All samples (loading: ca. 8 mg cm^{-2}) were supported with Au plate substrate (active geometrical surface: 0.25 cm^2). A potential–current curve of Pt black (TKK, Japan) is also plotted for comparison. Pt black loading is 0.06 mg/GC rod (ϕ5.2 mm). Highly active Zr-CNO was only shown in Fig. 2. For our oxide based catalysts, ORR activity at higher potential is insusceptible to effect of substance diffusion checking using static and RDE electrochemical system.[18,35] In this case, we can

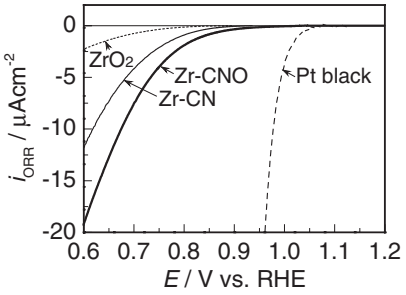

Figure 2. Voltammogram of Zr-CN/Au, Zr-CNO/Au, and ZrO_2/Au systems (DOO = 0.0, 0.83, 1.0) in 0.1 mol dm^{-3} at 30°C with scan rate of 5 mVs^{-1}. All samples were supported by Au plate (active geometrical surface: 0.25 cm^2). Pt black laoding: 0.06 mg/GC rod (ϕ5.2 mm).

see differences of ORR activity among catalysts by using Au plate as a substrate as well as our traditional system, even though observed current is smaller due to no mixing of carbon black as an electrical conducting additive.[18] The Zr-CN as a starting material and ZrO_2 seems to be still poor ORR activity. It makes no sense at all that there is no incessant interaction between catalysts and gold substrate. The Zr-CNOs with intermediate DOO values had a higher activity.

To elucidate the factors increasing the activity for the ORR, we will focus on the samples with higher range of DOO. In Figures 3a and 3b show the onset potential for the ORR, E_{ORR} (a), and the oxygen reduction reaction current, i_{ORR} at 0.85 V vs. RHE (b), for Zr-CNOs against higher range of DOO ($0.5 \leq DOO \leq 1.0$). E_{ORR} and i_{ORR} for ZrO_2 are also shown as references. For ZrO_2, it provides an interesting fact without carbon as a current corrector that E_{ORR} is prohibitively high even small i_{ORR}, indicating oxide have high capability for ORR catalyst. In a previous work, because the ZrO_2 indicated small ORR current, the onset potential E_{ORR} for ZrO_2 should be underestimated due to an overlap with both electrical double layer of additive carbon and irrelevant redox reaction like quinine/hydroquinone to the ORR. Both E_{ORR} and i_{ORR} for Zr-CNOs have a volcano-plot-like trend with a maximum at DOO = 0.83 vs. DOO ($0.5 \leq DOO \leq 1.0$).

Synchrotron X-ray diffraction with rietveld refinement.— Figure 4 shows X-ray powder diffraction of Zr-CN and Zr-CNOs with DOO of 0.54(a), 0.77(b), 0.83(c), 0.85(d), and 0.95(e). Monoclinic ZrO_2 phase was obviously observed in the partial oxidation under present condition. Cubic phase was also slightly observed at several spectra of Zr-CNOs. We can see that cubic/monoclinic ratio of ZrO_2 is almost linearly increases with increasing DOO as shown in the inset of Fig. 4. Next, we will look at minute change of crystalline structure

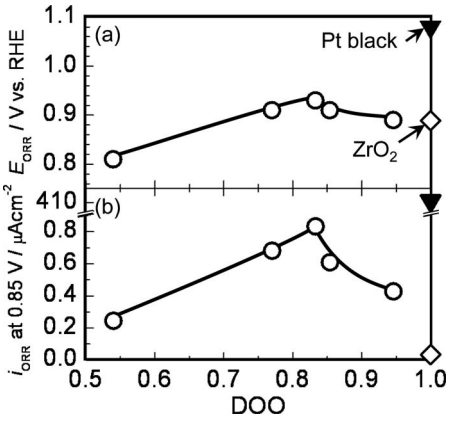

Figure 3. ORR onset potentials for Zr-CNO/Au plate (circle) and ZrO_2/Au (diamond) (a), ORR current i_{ORR} at 0.85 V vs. RHE (b). The trend of ORR activity seems to same behavior as with change of lattice parameter.

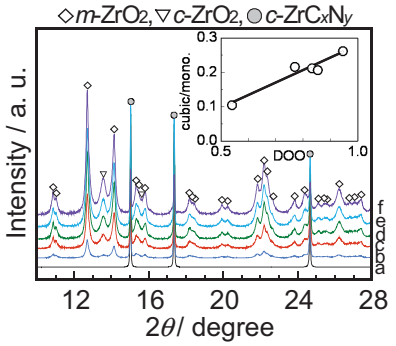

Figure 4. X-ray powder diffraction of Zr-CN and Zr-CNO with DOO = 0.54(a), 0.77(b), 0.83(c), 0.85(d), and 0.95(e). Wavelength of synchrotron X-ray was 0.70033 Å. Inset: Relationship between DOO and cubic/monoclinic ratio of ZrO_2. The cubic phase almost linearly increases with increases in DOO.

for the higher oxidation state ($0.5 \leq DOO \leq 1.0$) analyzed by using Rietveld refinement.

Lattice parameters of the catalysts depend on the concentration of free electrons via the deformation physical, chemical and electrical potentials of the occupied minima of the conduction bands. Figure 5 illustrates DOO-dependence of the lattice parameters: a_m, b_m, c_m and V_m of monoclinic ZrO_2 in Zr-CNO catalysts and stoichiometric ZrO_2 against DOO ($0.5 \leq DOO \leq 1.0$). The lattice parameter of a_m, b_m, c_m and V_m were decreased with increase in DOO up to 0.83, and became minimal value at DOO = 0.83. Over DOO = 0.83, the lattice parameters were drastically increased. The reference lattice parameters a_m, b_m, c_m and V_m of *m*-ZrO_2 are 5.1471(5) Å, 5.2125(4) Å, 5.3129(4) Å, and 140.70 $Å^3$ (JCPDS-ICDD 2009 card #37-1484). Comparing with the reference, the lattice parameters of Zr-CNO at DOO = 0.83 are significantly smaller.

Zirconium and oxygen site occupancies of *m*-ZrO_2 structure in Zr-CNOs were refined with Rietveld analysis as shown in Fig. 6. Figure 6 illustrates variations of the Zr, O(1) and O(2) site occupancies of monoclinic ZrO_2 in Zr-CNOs catalysts and stoichiometric ZrO_2 (diamond).

All of the site occupancy has a tendency to be convex downward against DOO and have a peak at DOO = 0.83 like the DOO variation

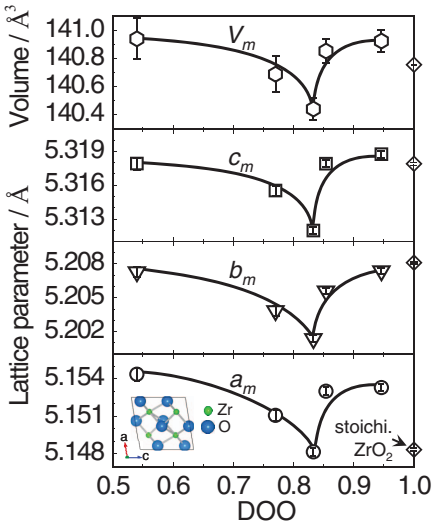

Figure 5. DOO-Dependence of the lattice parameters: a_m, b_m, c_m and V_m of monoclinic ZrO_2 in Zr-CNO catalysts and stoichiometric ZrO_2 (diamond). ZrO_2 was calcined at 900°C for 24 hour under pure oxygen using commercial ZrO_2. Inset: the crystal structure of monoclinic ZrO_2 [JCPDS-ICDD 2009 #37-1484].

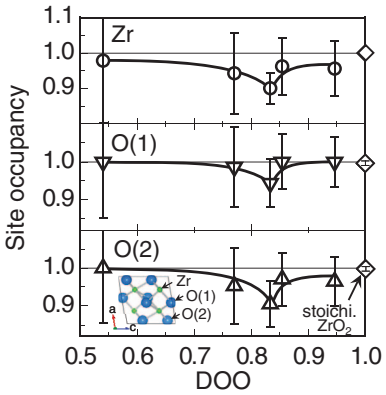

Figure 6. DOO variations of the Zr, O(1) and O(2) site occupancies in monoclinic ZrO_2 phase in Zr-CNO catalysts and stoichiometric ZrO_2 (diamond) against DOO. Inset: the crystal structure of monoclinic ZrO_2. At DOO = 0.83, oxygen and zirconium site occupancies significantly decreased related to stoichiometric ZrO_2.

of lattice parameters shown in Fig. 6. On the other hand, the oxygen site occupancy of Zr-CNO with DOO = 0.54 was at the same level as stoichiometric ZrO_2. On the contrary to this results, the lattice parameter for oxide seems to increase due to formation of defect such as oxygen vacancies with doping of rare earth oxides[31,32,40] or carbon and/or nitrogen.[31–33] We consider that this situation like increase in lattice parameter might limit to be caused by formation of only oxygen vacancy. For our sample, it is predicted from Rietveld refinement that Zr site occupancy might be decreased. Hence, the significant decrease in lattice parameter could be ascribed for the formation of oxygen and zirconium vacancies in monoclinic ZrO_2 phase. We easily guess that lattice parameters of monoclinic ZrO_2 bear a causal relationship to ORR activity of Zr-CNOs because lattice parameters and ORR activity have a volcano-, and reciprocal volcano-plot like tendency against DOO.

Here, formation of oxygen vacancies which could be in both cubic and monoclinic phase provokes a new question about major factor contributing toward improving of ORR activity. If the oxygen vacancy formed in cubic phase contributes to enhance ORR activity, the catalyst should indicate higher ORR activity at higher cubic/monoclinic phase ratio of ZrO_2 but in reality, it's not that way. Given the high onset potential E_{ORR} of ZrO_2 (only monoclinic phase) shown in Fig. 3a, we speculate that the oxygen vacancy formed in monoclinic phase have influence to enhance the ORR activity of our catalysts.

Cyclic voltammometry.— Cyclic voltammograms could help us understanding dramatic change in electrochemical active surface of sample. Figure 7 shows initial cyclic voltammograms of Zr-CN/Au plate, Zr-CNO/Au plate, and commercial ZrO_2/Au plate systems (DOO = 0.0, 0.83, 1.0) in 0.1 mol dm^{-3} at 30°C with scan rate of

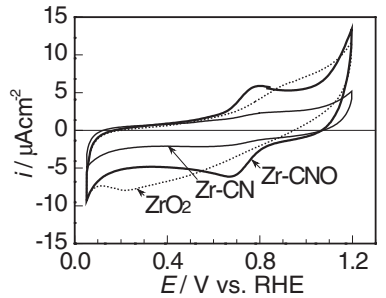

Figure 7. Initial cyclic voltammograms of Zr-CN/Au plate, Zr-CNO/Au plate (DOO = 0.0, 0.83, 1.0), and ZrO_2/Au systems in 0.1 mol dm^{-3} at 30°C with scan rate of 50 mVs^{-1}.

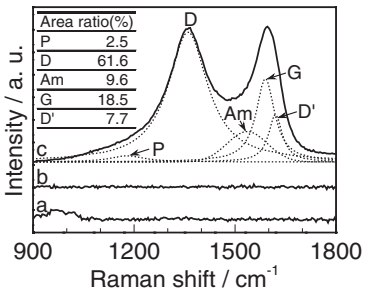

Figure 8. Raman spectra of Zr-CN(a), calcined ZrO_2(b) and Zr-CNO (DOO = 0.83)(c). Raman spectra of Zr-CNO was deconvoluted for five selected pristine carbons. The two main bands are the D ("Defect") band (Lorentzian at 1345–1360 cm^{-1}), the G band (Lorentzian at 1580–1600 cm^{-1}). Additional bands are attributed to: (i) amorphous carbon (Am band, Gaussian at 1490–1525 cm^{-1}), (ii) sp^3 carbon (P band, Lorentzian at 1150–1190 cm^{-1}) and (iii) another band accounting for structural disorder (D′ band, Lorentzian at −1620 cm^{-1}). Inset table shows area ratio by curve fitting for spectrum of Zr-CNO.

50 mVs^{-1}. There are redox peaks that correspond with surface functional group such as quinone/hydroquinone on carbon in CV of Zr-CNO/Au plate.[34] In contrast to CV of Zr-CNO/Au plate, no such redox peak was observed for Zr-CN and ZrO_2. Since no carbon species as a current corrector was contained in working electrodes, we can conclude the carbon should be precipitated on the surface of Zr-CNO catalysts during partial oxidation processes.

Raman spectroscopy.— Raman spectroscopy was performed to analyze structural properties of carbon which deposited on the surface. Figure 8 displays Raman spectra of Zr-CN (a), calcined ZrO_2 (b) and Zr-CNO (DOO = 0.83) (c). The penetration depth of laser is almost 1–2 μm in these samples. While there are significant peaks identified as carbon species in spectra for Zr-CNO, no peaks was observed in for Zr-CN and ZrO_2. Thus, the results of CV and Raman spectra, strongly suggest that the carbon deposited on the surface of Zr-CNO prepared from carbonitrides. To clarify the structural properties the deposited carbon, we further analyzed the Raman spectrum of Zr-CNO taking five kinds of pristine carbons into account.[41] The two main bands are the D ("Defect") band and the G ("Graphite") band. Additional bands are attributed to: (i) amorphous carbon (Am band), (ii) sp^3 carbon (P band) and (iii) another band corresponding to structural disorder (D' band). We can see sharp D band, G band, and amorphous band in the order corresponding to peak area ratio as shown in the inset of Fig. 8. Thus, the residual carbon on the surface of Zr-CNO was partially graphitized through partial oxidation.

Oxidation process analyzed by using TG.— Figure 9 shows TG curves of Zr-CN (a), partially oxidized Zr-CNO (DOO = 0.83 and 1.0)

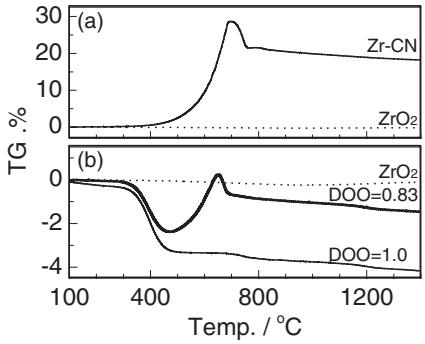

Figure 9. TG curves of non heat-treated Zr-CN (a), partially oxidized Zr-CNO (DOO = 0.83 and 1.0) (b) under pure O_2 (300 $mLmin^{-1}$) with rate of temperature increase of 20°$Cmin^{-1}$. Initial sample weight: ca. 20 mg.

(b) under pure O_2 (300 mLmin^{-1}) with rate of temperature increase of 20°Cmin^{-1}. Initial sample weight: ca. 20 mg. Stoichiometric ZrO_2 (reference sample) exhibited no change in weight as shown in Fig. 9a and 9b. In Fig. 9a, the weight gain of Zr-CN began at ca. 300°C, and reached at a peak maximum top at near 700°C (Zone 1: ~ 700°C), and then, decreased again above 700°C (Zone 2: 700°C ~). S. Shimada, et al. suggested that oxidation mechanism of ZrC single crystal as follows.[33,42] At early stage of the oxidation, amorphous ZrO_2/ZrO_{2-x} phase was formed in the vicinity of the ZrC layer. The oxide phase also contained some particle whose cubic ZrO_2 contained an un-oxidized carbon. As more oxidized, the surface oxide layer was linearly grown, and the carbon still remained in *c*-ZrO_2. Additionally, A. Bellucci et al. present the idea for carbon behavior that a relatively small fraction of carbon is burnt resulting from crack formation during the cooling treatment.[43] Thus, we suppose that the weight gain of Zr-CN at Zone 1 was due to turning to oxide, the latter abrupt weight decrease at Zone 2 was attributed to burning of precipitated carbon which observed in both CV curves and Raman spectra of Zr-CNO. The chemical equations during the above oxidation process are below.

$$\text{Zone 1}(\sim 700^\circ\text{C}): \ Zr_2CN + 4O_2 = 2ZrO_2 + 1/2N_2 \uparrow + C$$

$$\text{Zone 2}(700^\circ\text{C} \sim): \quad C + O_2 = CO_2$$

The oxidation processes of partially oxidized Zr-CNOs will become a little more complicated. For Zr-CNOs with intermediate DOO, the weight decrease was occurred until ca. 470°C, then TG curve of Zr-CNO varies similar to that of Zr-CN. In contrast to intermediate DOO, we can see step-like weight decrease in TG curve of DOO = 1 in Fig. 9b. This behavior could attribute to oxidation of the deposited carbon on the surface of catalysts. Beyond ca. 470°C, oxidation process of intermediate Zr-CNO might be similar to the TG curve of Zr-CN. The weight change around peak at 650°C in Fig. 9b should result from oxidation of residual Zr-CN inside Zr-CNO powder. Therefore, it became apparent from results of CV, Raman and TG analyzes that the carbon which originating in Zr-CN was precipitated on the surface of Zr-CNO during partial oxidation.

On the other hand, from peak fitting of Raman spectra, we estimated co-existing of some types of carbon such as graphite and amorphous which deposited on the surface of Zr-CNO during heat-treatment. P. M. Ajayan et al. reported that oxidation temperature of carbon depends on the type of carbon, and specific carbon state rapidly burn like ignition.[44–46] Hence, there is a possibility that specific types of carbon on the surface of Zr-CNO rapidly burn under certain specified conditions, functioning a strongly reducing agent to oxide on the surface. In TG curve of DOO = 1 in Fig. 9b, the presence of step-like weight decrease could support co-existing of some types of morphologically-different carbons because morphologically-different carbon like graphite, amorphous carbon different its burning temperature. Additionally, nature of the carbon might vary depending on types of the carbon that act as strong reducing agency or electrically conductive agency on the surface.

Surface composition ratio by using XPS.— X-ray photoelectron spectroscopy (XPS) was performed to analyze with the composition ratio on the surface (escape depth of photoelectron: ~ ca. 5 nm) of Zr-CNO. Figure 10 shows surface composition ratios, O/Zr, C/Zr and N/Zr of Zr-CNO and stoichiometric ZrO_2. Stoichiometric ZrO_2 was shown as a reference. Carbon on the surface of stoichiometric ZrO_2 is identified as free carbon in XPS chamber because ZrO_2 was calcined under pure oxygen for 24 hours.

C/Zr curve is convex downward with DOO. Remarkably, relative amount of the carbon for the Zr-CNO with DOO = 0.83 is very low at same level or lower level compared with that of carbon for the stoichiometric ZrO_2. However, the carbon was significantly observed in CVs in Fig. 7 and Raman spectrum in Fig. 8 at deeper detection depth related to the depth of XPS analysis. Thus, it become apparent that the carbon was not remained on top of the surface but under the surface concerning high ORR active Zr-CNO with DOO = 0.83. For

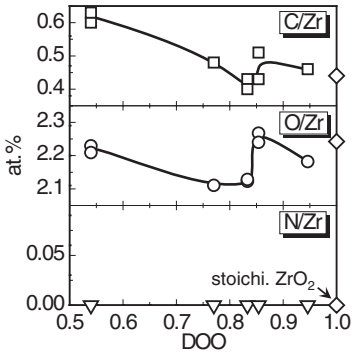

Figure 10. Composition ratio on surface of Zr-CNO and stoichiometric ZrO_2 against DOO.

Zr-CNO with DOO = 0.54, while, there are much carbon without its oxidation during heat-treatment. Excess deposited carbon (without act as reducing agency) on the surface could block active site for the ORR because ZrO_2 indicate higher onset potential. Therefore, the active site could not exist on the carbon but oxide.

Drastic change of O/Zr ratio around DOO = 0.83 occur in connection with decrease in C/Zr ratio at same time. From TG analysis as discussed above, we predict the effects of precipitated carbon act as strong reducing agent on the surface. Hence, significant decrease in both carbon and oxygen on the surface of Zr-CNO could support our prediction.

ORR current versus formed oxygen vacancy.— We predict that oxygen vacancy was formed due to the function of deposited carbon act as strong reducing agency. In particular, high ORR active Zr-CNO has more high concentration of the vacancy on the surface of Zr-CNO. Figure 11 shows correlation between the ORR current, i_{ORR} at 0.85 V vs. RHE and oxygen composition ratio on surface (a), and sum of oxygen site occupancies in *m*-ZrO_2 phase (b). Concentration of oxygen vacancy increases with shift to right in abscissa axis. It is clear that ORR current at 0.85 V increase with increase in concentration of oxygen vacancy on the surface and structure shown in Figs. 11a and 11b. Therefore, the amount of oxygen vacancy was directly involved in improving ORR activity, leading to provide a function of the oxygen vacancy as ORR active site.

Considering oxidation process of ZrC single crystal,[33,42,43] cubic ZrO_2 which could contain the carbon from starting material should

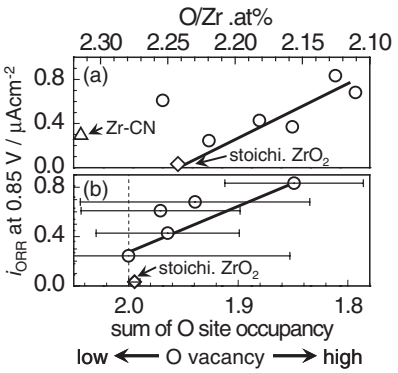

Figure 11. Correlation between the ORR current, i_{ORR} at 0.85 V vs. RHE and oxygen composition ratio on the surface of Zr-CNO (a), and sum of oxygen site occupancy in monoclinic ZrO_2 phase (b). Decrease in the composition ratio and sum of the occupancy should indicate increase in concentration of oxygen vacancies for Zr-CNO. The ORR current had a strong correlation with concentration of the oxygen vacancies on the surface and in monoclinic ZrO_2 structure.

present on the surface of the sample. In inset of Fig. 2, the cubic/monoclinic phase ratio increases with increasing in monoclinic phase. If improvement of the ORR activity mainly depends on oxygen vacancies that formed in the cubic phase, catalysts will exhibit the largest ORR activity at higher DOO. However, this is not the case. It elucidate from the electrochemical measurement for ZrO_2/Au that its phase of ZrO_2 is consisted of only monoclinic ZrO_2 indicated high onset potential for the ORR. From this result, we conclude that oxygen vacancy formed in monoclinic (not cubic) ZrO_2 could act as ORR active site.

Conclusions

Partially oxidized zirconium carbonitrides were investigated as a non-precious metal cathode for PEFCs. The Zr-CN powder was heat-treated at 1000°C for 20 hours under controlling oxygen partial pressure P_{O2} from 10^{-2} to 10^{-18} atm. To estimate ORR activity without contribution from carbon additives, we used a gold plate as a substrate. It is clear that the onset potential of Zr-CNO catalysts is very higher than previously reported values (with conducting carbon), though the ORR current is lower than catalyst mixed with carbon. The ORR activity for Zr-CNOs have a volcano-plot–like tendency with maximum at DOO = 0.83 versus DOO.

For the high ORR active Zr-CNO (DOO = 0.83), the significant decrease in lattice parameter and Zr and O occupancies were revealed with Rietveld refinement. The significant decrease in lattice parameter could be ascribed for the formation of oxygen and zirconium vacancies in monoclinic ZrO_2 phase.

It is elucidated from the results of CV, Raman, TG analyzes that carbon which originated in Zr-CN as starting material deposited on the surface of Zr-CNO during partial oxidation process. However, there is almost no carbon on the end surface of high ORR active Zr-CNO (DOO = 0.83) analyzed by using XPS. At the same time, the oxygen contents on the surface was specifically decreased with regard to only high ORR active Zr-CNO (DOO = 0.83). On the other hand, during partial oxidation process, the deposited carbon on the surface of Zr-CNO should oxidize as revealed by the TG analysis. We recognized five type of carbon: graphite with and without defect, amorphous, sp^2, sp^3 analyzed with curve fitting of Raman spectra for Zr-CNO. Such carbons could act as strong reducing agency on the surface and promote oxygen-vacancy formation on Zr-CNOs. In addition, we think that such carbons also might act as current corrector. However, exceed deposited on the surface of Zr-CNO could block the ORR active site, estimating from result of large amount of the deposited carbon on the surface of low ORR active Zr-CNO.

During oxidation process, cubic ZrO_2 that include the carbon might form on the surface of Zr-CNO catalysts, considering from oxidation process of ZrC single crystal. Oxygen vacancies should form in both cubic and monoclinic phase. If the oxygen vacancy formed in cubic phase contributes to enhance ORR activity, the Zr-CNO should indicate higher ORR activity at higher cubic phase ratio of ZrO_2. However, high ORR active point is not at a maximum of cubic phase ratio. Meanwhile, given the high onset potential of ZrO_2 (only monoclinic phase), we speculate that the oxygen vacancy formed in monoclinic phase have influence to enhance the ORR activity of our catalysts. In fact, the ORR current had a strong correlation with concentration of the oxygen vacancies on the surface and in monoclinic ZrO_2 structure. From these results, thus, we consider that the oxygen vacancies which not form in cubic phase but form in monoclinic phase could be act as active sites for the ORR.

Acknowledgments

The synchrotron radiation experiments were conducted with the approval of the Japan Synchrotron Radiation Research Institute (Proposal Nos. 2009B1824, 2010A1750 and 2010B1793, 2010B1887). We thank A.L.M.T. Corp. for supplying the Zr-CN, and Prof. M. Tachibana in Yokohama City University for highly value your input in Raman spectroscopy. This work was supported by grant-in-Aid for JSPS Fellow and the New Energy and Industrial Technology Development Organization (NEDO).

References

1. R. J. Jasinski, *Nature*, **201**, 1212 (1964).
2. O. Contamin, C. Debiemme-Chouvy, M. Savy, and G. Scarbeck, *J. New Mater. Electrochem. Syst.*, **3**, 67 (2000).
3. P. Convert, C. Coutanceau, P. Crouigneau, F. Gloaguen, and C. Lamy, *J. Appl. Electrochem.*, **31**, 945 (2001).
4. P. Gouerec and M. Savy, *Electrochim. Acta*, **44**, 2653 (1999).
5. N. Alonso-Vante and H. Tributsch, *Nature*, **323**, 431 (1986).
6. H. Tributsch, *Catal. Today*, **39**, 177 (1997).
7. N. Alonso-Vante, I. V. Malakhov, S. G. Nikitenko, E. R. Savinova, and D. I. Kochubey, *Electrochim. Acta*, **47**, 3807 (2002).
8. D. Cao, A. Wieckowski, J. Inukai, and N. Alonso-Vante, *J. Electrochem. Soc.*, **153**, A869 (2006).
9. M. Chokai, M. Taniguchi, S. Moriya, K. Matsubayashi, T. Shinoda, Y. Nabae, S. Kuroki, T. Hayakawa, M. Kakimoto, J. Ozaki, and S. Miyata, *J. Power Sources*, **195**, 5947 (2010).
10. E. J. Biddinger and U. S. Ozkan, *J. Phys. Chem. C*, **114**, 15306 (2010).
11. G. Liu, X. Li, P. Ganesan, and B. N. Popov, *Electrochim. Acta*, **55**, 2853 (2010).
12. G. Lalande, R. Cote, G. Tamizhmani, D. Guay, J. P. Dodelet, L. Dignard-Bailey, L. T. Weng, and P. Bertrand, *Electrochim. Acta*, **40**, 2635 (1995).
13. J. Maruyama and I. Abe, *Chem. Mater.*, **17**, 4660 (2005).
14. E. Proietti, S. Ruggeri, and J.-P. Dodelet, *J. Electrochem. Soc.*, **155**, B340 (2008).
15. A. Garsuch, K. MacIntyre, X. Michaud, D. A. Stevens, and J. R. Dahn, *J. Electrochem. Soc.*, **155**, B953 (2008).
16. X. G. Li, G. Liu, and B. N. Popov, *J. Power Sources*, **195**, 6373 (2010).
17. G. Liu, X. Li, J.-W. Lee, and B. N. Popov, *Catal. Sci. Technol.*, **1**, 207 (2011).
18. Y. Ohgi, A. Ishihara, K. Matsuzawa, S. Mitsushima, and K. Ota, *J. Electrochem. Soc.*, **157**, B885 (2010).
19. A. Ishihara, Y. Ohgi, K. Matsuzawa, S. Mitsushima, and K. Ota, *Electrochim. Acta*, **55**, 8005 (2010).
20. Y. Ohgi, A. Ishihara, Y. Shibata, S. Mitsushima, and K. Ota, *Chem. Lett.*, **37**, 608 (2008).
21. Y. Maekawa, A. Ishihara, J.-H. Kim, S. Mitsushima, and K. Ota, *Electrochem. Solid-State Lett.*, **11**, B109 (2008).
22. A. Ishihara, Y. Shibata, S. Mitsushima, and K. Ota, *J. Electrochem. Soc.*, **155**, B400 (2008).
23. A. Ishihara, S. Doi, S. Mitsushima, and K. Ota, *Electrochim. Acta*, **53**, 5442 (2008).
24. Y. Shibata, A. Ishihara, S. Mitsushima, N. Kamiya, and K. Ota, *Electrochem. Solid-State Lett.*, **10**, B43 (2007).
25. G. Balducci, J. Kaspar, P. Fornasiero, M. Graziani, M. S. Islam, and J. D. Gale, *J. Phys. Chem. B*, **101**, 1750 (1997).
26. J. Kaspar, P. Fornasiero, and M. Graziani, *Catal. Today*, **50**, 285 (1999).
27. M. Yashima, M. Kakihana, and M. Yoshimura, *Solid State Ionics*, **86-88**, 1131 (1996).
28. M. Ozawa, M. Kimura, and A. Isogai, *J. Alloys Compd.*, **193**, 73 (1993).
29. E. C. Subbarao, H. S. Maiti, and K. K. Srivastava, *Phys. Status Solidi A*, **21**, 9 (1974).
30. J. Chevalier, L. Gremillard, A. V. Virkar, and D. R. Clarke, *J. Am. Ceram. Soc.*, **92**, 1901 (2009).
31. M. Lerch and O. Rahaeuser, *J. Mater. Sci.*, **32**, 1357 (1997).
32. R. Collongues, J. C. Gilles, A. M. Lejus, M. Perez Jorba, and D. Michel, *Mater. Res. Bull.*, **2**, 837 (1967).
33. S. Shimada, M. Nishisako, M. Inagaki, and K. Yamamoto, *J. Am. Ceram. Soc.*, **78**, 41 (1995).
34. K. Kinoshita and J. A. S. Bett, *Carbon*, **11**, 403 (1973).
35. Y. Ohgi, A. Ishihara, K. Matsuzawa, S. Mitsushima, K. Ota, M. Matsumoto, and H. Imai, *Electrochim. Acta*, **68**, 192 (2012).
36. H. M. Rietveld, *J. Appl. Crystallogr.*, **2**, 65 (1969).
37. F. Izumi and K. Momma, *Solid State Phenom*, **130**, 15 (2007).
38. K. Momma and F. Izumi, *J. Appl. Crystallogr.*, **41**, 653 (2008).
39. A. Sadezky, H. Muckenhuber, H. Grothe, R. Niessner, and U. Poeschl, *Carbon*, **43**, 1731 (2005).
40. S. Somiya, N. Yamamoto, and H. Yanagida, *Advances in Ceramics*, Vol. 24A: Science and Technology of Zirconia III, American Ceramic Society, Westerville, OH (1988).
41. F. Charreteur, F. Jaouen, S. Ruggeri, and J.-P. Dodelet, *Electrochim. Acta*, **53**, 2925 (2008).
42. S. Shimada, *Solid State Ionics*, **141-142**, 99 (2001).
43. A. Bellucci, D. Gozzi, T. Kimura, T. Noda, and S. Otani, *Surf. Coat. Technol.*, **197**, 294 (2005).
44. P. M. Ajayan, T. W. Ebbesen, T. Ichihashi, S. Iijima, K. Tanigaki, and H. Hiura, *Nature*, **362**, 522 (1993).
45. S. C. Tsang, P. J. F. Harris, and M. L. H. Green, *Nature*, **362**, 520 (1993).
46. P. M. Ajayan, M. Terrones, A. de la Guardia, V. Huc, N. Grobert, B. Q. Wei, H. Lezec, G. Ramanath, and T. W. Ebbesen, *Science*, **296**, 705 (2002).